THE ANATOLIAN JOURNAL OF CARDIOLOGY

Official journal of the TURKISH SOCIETY OF CARDIOLOGY

LncRNA Growth Arrest Specific 5 Promotes Glucose Metabolism Reprogramming Via the IGF2BP1/SIX1 Axis and Inhibits Ferroptosis of Endothelial Progenitor Cells Via the miR-23a-3p/SLC7A11 Axis in Coronary Heart Disease

ABSTRACT

Background: Growth arrest specific 5 (GAS5) is a long noncoding RNA (lncRNA) that regulates the function of cardiovascular cells in various cardiovascular diseases. The current study delved into the regulation of GAS5 on the function of endothelial progenitor cells (EPCs) and its potential regulatory mechanism in coronary heart disease (CHD).

Methods: Reverse transcription-quantitative polymerase chain reaction was used to detect GAS5 expression in the blood samples and EPCs from CHD patients and healthy controls. Cell Counting Kit-8, colony formation, flow cytometry, and transwell assays were performed to evaluate cell phenotype of EPCs. Ferroptosis was detected by the measurement of Fe2+, malondialdehyde, GSH, and reactive oxygen species (ROS) levels. Glycolysis was determined by extracellular acidification rate (ECAR), oxygen consumption rate (OCR), glucose uptake and lactate production.

Results: Growth arrest specific 5 was downregulated in the blood samples and EPCs from CHD patients. Growth arrest specific 5 deficiency suppressed EPC proliferative capacity, migration, invasion and facilitated EPC apoptosis while GAS5 overexpression showed contrary effects. Moreover, GAS5 silencing inhibited the glucose metabolic reprogramming, as evidenced by the reduced ECAR, glycolysis capacity, ATP, glucose uptake and lactate production, and elevated OCR. Additionally, GAS5 overexpression attenuated the erastin-induced ferroptosis of EPCs. Growth arrest specific 5 could bind to IGF2BP1 to enhance the mRNA stability of glycolysis transcriptional regulator SIX1. Growth arrest specific 5 interacted with miR-23a-3p to regulate SLC7A11 expression. GAS5 promoted glucose metabolic reprogramming of EPCs by upregulating SIX1 and inhibited EPC ferroptosis by elevating SLC7A11.

Conclusion: Growth arrest specific 5 promotes glucose metabolic reprogramming and represses ferroptosis of EPCs via the IGF2BP1/SIX1 and miR-23a-3p/SLC7A11 dual-regulatory pathways in CHD.

Keywords: Coronary heart disease, ferroptosis, GAS5, glucose metabolic reprogramming, long noncoding RNA

INTRODUCTION

Coronary heart disease (CHD) caused by coronary atherosclerosis is a common cause of heart attack. Clinically, patients with CHD exhibit symptoms such as angina pectoris induced by temporary myocardial ischemia. According to the China Cardiovascular Health and Disease Report 2022, there are an estimated 330 million people with cardiovascular diseases in China, among which 11.39 million cases are CHD.[1] The high incidence and mortality rate of CHD pose a high burden to society. Currently, the treatment of CHD mainly includes percutaneous coronary intervention, bypass surgery, and pharmacological therapy. However, many patients are not allowed to receive interventional procedures, and for those receiving treatment, the clinical outcomes are limited by myocardial damage and subsequent heart failure.[2] The exploration of novel effective therapeutic strategies is still in urgent need.

ORIGINAL INVESTIGATION

Ming Zhong[1,2]
Wenxia Xu[3]
Biao Tang[2]
Qiang Zhao[2]
Zenan Jiang[2]
Yinfeng Liu[1]

[1]*Department of Cardiology, Heart Center, Zhujiang Hospital of Southern Medical University, Guangzhou, Guangdong, China*
[2]*Department of Cardiology, Jinhua Municipal General Hospital, Jinhua, Zhejiang, China*
[3]*Central Laboratory, Jinhua Municipal General Hospital, Jinhua, Zhejiang, China*

Corresponding author:
Yinfeng Liu
✉ Ucce44598232@outlook.com

Received: December 1, 2024
Accepted: December 20, 2024
Available Online Date: March 4, 2025

Cite this article as: Zhong M, Xu W, Tang B, Zhao Q, Jiang Z, Liu Y. LncRNA growth arrest specific 5 promotes glucose metabolism reprogramming via the IGF2BP1/SIX1 axis and inhibits ferroptosis of endothelial progenitor cells via the miR-23a-3p/SLC7A11 axis in coronary heart disease. *Anatol J Cardiol.* 2025;29(4):181-192.

DOI:10.14744/AnatolJCardiol.2025.5042

Endothelial dysfunction is closely associated with the onset of CHD.[3] Endothelial progenitor cells (EPCs) can differentiate into mature endothelial cells and are considered as critical contributors to neovascularization and vascular repair, showing the potential for CHD therapy.[4] Studies have demonstrated that EPCs facilitate the vascular remodeling of ischemic and damaged tissues in animal models and human cases of ischemia.[5,6] However, the transplantation of EPCs is challenged by the number, function, and aging.[7] It is essential to develop effective strategies to improve the survival of EPCs in the recipient.

Long noncoding RNAs (lncRNAs) are noncoding transcripts over 200 nucleotides long and possess no protein-coding ability.[8,9] They are crucial regulators of gene expression at epigenetic, transcriptional, and post-transcriptional levels.[10] The regulatory mechanisms of lncRNAs include chromatin remodeling, pre-mRNA splicing, mRNA translation, and microRNAs (miRNAs) sponging. Increasingly, studies have shown that numerous lncRNAs are aberrantly expressed in various diseases including cardiovascular diseases. For example, lncRNA uc003pxg.1 facilitates endothelial cell proliferative capacity and migration ability by regulating miR255p in coronary artery disease.[11] Long noncoding RNAs NEAT1 suppressed the survival of human coronary endothelial cells (HCAECs) and induced cell apoptosis via the miR-140-3p/MAPK1 axis in coronary atherosclerotic heart disease.[12] Growth arrest specific 5 (GAS5) is indicated to be related to the progression of cardiovascular diseases. For example, GAS5 is reported to protect against the norepinephrine-induced cardiomyocyte apoptosis by downregulating sema3a in myocardial infarction.[13] Growth arrest specific 5 silencing is revealed to inhibit the proliferative capacity and senescence of endothelial progenitor cells by regulating the miR-223/NAMPT axis and the PI3K/AKT pathway.[14] Growth arrest specific 5 also regulates the senescence of vascular smooth muscle cells by sponging miR-665 to upregulate SDC1.[15] In the previous study, GAS5 was preliminarily found to participate in the progression of CHD by regulating the function of EPCs through the miR-495-3p/SIX1 and IGF2BP2/NRF2 dual-regulatory pathways.[16] However, the specific molecular mechanism by which GAS5 regulates the function of EPCs still needs further exploration.

HIGHLIGHTS

- Growth arrest specific 5 contributes to the growth, migration and invasion of endothelial progenitor cells.
- Growth arrest specific 5 promoted the glucose metabolic reprogramming of endothelial progenitor cells by upregulating SIX1.
- Growth arrest specific 5 inhibits ferroptosis of endothelial progenitor cells by upregulating SLC7A11.
- Growth arrest specific 5 interacts with IGF2BP1 to stabilize SIX1.
- Growth arrest specific 5 binds to miR-23a-3p to upregulate SLC7A11 in EPCs.

This study intended to investigate the role of the novel molecular mechanism of GAS5 in CHD. It was hypothesized that GAS5 affected CHD progression by regulating the function of EPCs via upregulating the expression of the ferroptosis inhibitor SLC7A11 and the glycolysis transcriptional regulator SIX1, which might provide novel insight into CHD therapy.

METHODS

Patient Sample Collection

The atherosclerotic peripheral blood (2 mL) was collected from 30 CHD patients and 30 healthy individuals in ethylenediaminetetraacetic acid (EDTA) tubes in our hospital. The plasma was collected after centrifugation for 15 minutes at 3000 rpm at 4°C and then stored at −80°C for further analysis. All participants have signed the informed consent. The Ethics Committee of our hospital has approved this study.

Isolation and Incubation of Endothelial Progenitor Cells

Peripheral blood from CHD patients and healthy individuals were collected and diluted with phosphate buffer saline (PBS). Next, the isolation of peripheral blood mononuclear cells (PBMCs) was conducted with ficoll density gradient centrifugation, followed by washing and centrifugation to remove the platelet. The supernatant was removed and PBMCs were resuspended in culture medium to adjust a concentration at 1×10^6. Next, cells were cultured on 6-well plates coated with fibronectin, and each well was added with 2 mL EGM-2 (LONZA, USA) and maintained at 37 °C with 95% air and 5% CO_2.

After culturing for 4 days, to select EPCs, the plates were washed with PBS for removing the non-attached cells. The attached cells were collected and subject to flow cytometry analysis with for surface markers including CD34, CD31, and CD45.[17]

Cell Transfection

Two specific siRNAs targeting GAS5 (si-GAS5#1/#2) and negative control (si-NC), SIX1 and IGF2BP1 overexpression vector and pcDNA3.1 empty vector (oe-NC), miR-23a-3p mimic and NC mimic were designed and synthesized by GenePharma (Shanghai, China). The transfection vector or plasmid was conducted with Lipofectamine 3000 (Invitrogen, Carlsbad, CA, USA) for 48 hours.

Reverse Transcription-Quantitative Polymerase Chain Reaction

Total RNA was extracted using TRIzol reagent. A High-Capacity cDNA Reverse Transcription Kit (Applied Biosystems, USA) was applied for synthesizing cDNAs. Quantitative polymerase chain reaction was carried out with a LightCycler FastStart DNA MasterPLUS SYBR Green I mix (Roche, Germany) on the ABI-7500 platform. Gene expression was calculated with the $2^{-\Delta\Delta Ct}$ method, and β-actin and U6 served as internal references.

Western Blot

Radioimmunoprecipitation assay lysis buffer was used for total protein collection. A Bicinchoninic Acid Kit was adopted for the detection of protein concentration. Next,

the protein sample was electrophoresed by SDS–polyacrylamide gel electrophoresis (Bio-Rad, USA) and electrotransferred to nitrocellulose membranes. Subsequently, 5% skim milk was applied for blocking these membranes, which were then incubated overnight with the primary antibodies at 4°C, with β-actin as a loading control. After rinsing with Tris-Borate-Sodium Tween-20 (TBST), the membranes were incubated with a secondary antibody for 60 minutes. The enhanced chemiluminescence (Pierce, USA) was used for the visualization of protein signals.

Fluorescent In Situ Hybridization

Fluorescent In Situ Hybridization Kit (RiboBio, Guangzhou, China) was used to determine the subcellular localization of GAS5 following the producer's protocol. Endothelial progenitor cells were seeded in slides, processed with 4% paraformaldehyde, rinsed with PBS, and processed using 0.5% Triton X-100. Subsequently, EPCs were hybridized with probes for GAS5 and IGF2BP1 (RiboBio, China) overnight at 37 °C. 4′,6-diamidino-2-phenylindole (DAPI) was applied to stain the nucleus. The images were captured by a confocal fluorescence microscope (Leica, Wetzlar, Germany).

Co-Immunoprecipitation

Endothelial progenitor cells were treated using lysis buffer, centrifuged, and the supernatant was incubated with anti-IgG or anti-SIX1 overnight at 4°C. Next, the mixture was captured by incubation with protein A/G agarose beads for 4 hours. After washing with ice-cold IP buffer, the samples were centrifuged at 1000 × *g* for 2 minutes to remove the supernatant. Subsequently, the proteins were separated from beads using an immunoblotting loading buffer. The supernatant was harvested and the level of binding proteins was subjected to Western blot.

RNA Immunoprecipitation

Endothelial progenitor cells were lysed and the lysate was incubated with anti-IgG (negative control) or anti-Ago2 antibody conjugated with magnetic beads at 4°C overnight. The beads were collected and washed, followed by proteinase K treatment. RNA extraction from the complex was conducted using phenol: chloroform: isoamyl alcohol solution. Immunoprecipitated RNAs from anti-IgG or anti-Ago2 were subject to reverse transcription-quantitative polymerase chain reaction (RT-qPCR) analysis.

RNA Pull-Down

Biotinylated GAS5, miR-23a-3p, and control NC probes were provided by Ribobio. Endothelial progenitor cells were lysed and incubated overnight with biotinylated probes-conjugated with magnetic beads at 4°C. After collecting and washing beads, the RNA or protein in the complex was purified. The enrichment of IGF2BP1, miRNAs, or SLC7A11 was subject to western blot or RT-qPCR analysis.

Dual-Luciferase Reporter Assays

Growth arrest specific 5 and SLC7A11 3′UTR containing including wild-type (Wt) and mutated (Mut) binding sequence with miR-23a-3p were subcloned into pmirGLO vector (Promega, USA) for the construction of GAS5-wt/mut or SLC7A11-wt/mut vector. The vector was co-transfected in EPCs with miR-23a-3p/NC mimic for 48 hours. The luciferase activities were determined with a Promega dual-luciferase reporter kit.

Cell Viability

The viability of EPCs was detected using CCK-8 assays. Briefly, EPCs were seeded in 96-well plates (5×10^3 cells in each well) and cultured for indicated time (1, 2, 3, 4 days). EPCs in each well were supplemented with 10 μL CCK-8 reagent and cultured for 120 minutes. The absorbance was analyzed at 450 nm.

Colony Formation Assay

Endothelial progenitor cells were seeded in 6-well plates at 500 cells per well. After a 2-week incubation, 4% polyformaldehyde was applied to fasten colonies, which were then dyed by 0.5% crystal violet for 1 hour. The colony number was finally calculated with a microscope.

Flow Cytometry Analysis

The apoptosis of EPCs was measured using an Annexin V-FITC/PI Apoptosis Kit (Mutisiences, China) following the producer's guide. Endothelial progenitor cells after transfection were harvested, and stained with Annexin V-FITC and Propidium Iodide for 20 minutes at 4°C in darkness. Cell apoptotic rate was evaluated by FACScan Flow Cytometer, BD Biosciences, USA) and analyzed with FlowJo software.

Transwell Assays

The transwell assays were performed for evaluating the migration and invasion abilities of EPCs using Transwell chambers (Costar, USA) coated with or without matrigel (BD Biosciences, USA). Endothelial progenitor cells (5×10^4) were suspended in culture medium (0.5 mL) containing 0.1% bovine serum albumin and added in the top Transwell chambers, and culture media with 20% FBS in the lower chambers. The incubation last for 24 hours. After PBS washing, and processing in 4% paraformaldehyde, EPCs were stained for 5 minutes with crystal violet solution. The migrated or invaded cells were counted and imaged with an inverted microscope.

Glucose Uptake Measurement

Endothelial progenitor cells were grown into 96-well plates at 1×10^4 cells/well, and incubated at 37°C overnight. Next, EPCs were deprived of sugar for 2 hours. Then each well was supplemented with 10 μL 2-deoxy-d-glucose (2-DG) and cultured for 20 minutes. The glucose intake was determined at 412 nm wavelength.

Lactic Acid Production Assay

The production of lactic acid in EPCs was assessed using an L-lactic acid test kit (colorimetry). Endothelial progenitor cells were first grown in 96-well plates and cultured overnight at 37°C. After starvation for 120 minutes, the supernatant was harvested and lactic acid production was evaluated at 450 nm.

Extracellular Acidification Rate and Oxygen Consumption Rate Measurement

Endothelial progenitor cells were grown in 96-well plates added with 10% FBS and cultured at 37°C overnight. After measuring the baseline concentration, glucose, oligomycin,

and 2-DG were supplemented into each well successively for extracellular acidification rate (ECAR) measurement. For oxygen consumption rate (OCR) measurement, oligomycin, FCCP, antimycin A, and rotenone were added successively. The results were analyzed using XF-96Wave software.

Malondialdehyde Detection

The malondialdehyde (MDA) content in the lysate of EPCs was detected using a Lipid Peroxidation Assay Kit (Abcam, UK) based on the manufacturer's protocol. Briefly, EPCs after erastin treatment and indicated transfection were harvested and lysed, and subsequently centrifuged for 10 minutes at 13 000 × *g* for removing the insoluble material. Then thiobarbituric acid (TBA) solution was supplemented to well-containing samples and MDA standards, incubated at 95°C for 1 hour, cooled in an ice bath for 10 minutes, and transferred to wells of the microplate. The absorbance is measured at 532 nm with a microplate reader.

Glutathione (GSH)/oxidized glutathione (GSSG) Detection

The level of GSH/GSSG in EPCs was measured using a GSH and GSSG Assay Kit (Beyotime, China) based on the producer's guide. The resulting mixture was measured using a microplate reader at 412 nm. The GSH level is calculated as GSH = Total Glutathione−GSSG × 2.

Iron Assay

Intracellular ferrous iron (Fe^{2+}) level in EPCs was detected using an iron assay kit (Abcam, UK) following the manufacturer's protocol. Endothelial progenitor cells were grown in a culture plate and exposed to erastin for 12 hours. Then cells were harvested, washed, and homogenized in iron assay buffer, followed by for 10-minute centrifugation at 4°C. Next, the supernatant was harvested and supplemented iron reducer into each well, mixed, and incubated for 30 minutes at ambient temperature. Subsequently, the iron probe was supplemented and mixed, followed by a 1-hour incubation in darkness. Finally, a colorimetric microplate reader was applied for absorbance detection at 593 nm.

Statistical Analysis

GraphPad Prism software (GraphPad Software Inc., San Diego, CA) was used for statistical analysis. The experiments were independently conducted at least 3 times. The normality of data distribution was evaluated with the Shapiro–Wilk test. Data were presented as the mean ± SD. Two-tailed Student's *t* test was used for comparison between 2 groups, and one-way analysis of variance followed by Tukey's post hoc test or two-way analysis of variance followed by Bonferroni's post hoc test was applied for comparison among multiple groups. Pearson correlation analysis was used to evaluate the expression correlation between genes. *P* value less than .05 indicated statistical significance.

RESULTS

Growth Arrest Specific 5 is Downregulated in Coronary Heart Disease and Accelerates Endothelial Progenitor Cell Proliferation, Migration, and Invasion

The GAS5 level was determined in the blood samples and EPCs collected from CHD patients (n = 30) and healthy individuals (n = 30). The results of RT-qPCR analysis identified that GAS5 was downregulated in both blood samples and EPCs of CHD patients compared with healthy controls (Figure 1A and B), suggesting its association with CHD progression and behaviors of EPCs. Next, The effects of GAS5 on EPC growth were investigated. The si-GAS5#1/2 or pcDNA3.1/GAS5 vector was transfected into EPCs to establish GAS5-silenced or overexpressed EPCs. The knockdown and overexpression efficiency of GAS5 was validated by RT-qPCR analysis (Figure 1C and D). Cell Counting Kit-8 assays demonstrated that GAS5 knockdown significantly decreased the viability of EPCs while GAS5 overexpression evidently enhanced EPC growth (Figure 1E and F). Consistently, colony formation assays showed that GAS5 silencing reduced the colony number of EPCs while GAS5 overexpression showed the contrary effects (Figure 1G and H). Based on flow cytometry analysis, GAS5 silencing induced a significant increase in the apoptotic rate of EPCs, while GAS5 overexpression significantly inhibited EPC apoptosis (Figure 1I and J). Furthermore, transwell assays demonstrated that migration and invasion of EPCs were repressed in response to GAS5 silencing, and enhanced in response to GAS5 overexpression (Figure 1K-N). Overall, GAS5 contributes to EPC growth, migration, and invasion in vitro.

Growth Arrest Specific 5 is Located in the Cell Cytoplasm of Endothelial Progenitor Cells

To determine the subcellular localization of GAS5 in EPCs, Fluorescence *in situ* hybridization (FISH) assays were conducted, and the results demonstrated the main distribution of GAS5 in the cell cytoplasm of EPCs (Figure 2A). Consistently, the results of subcellular fractionation assays also revealed that GAS5 was located in the cell cytoplasm of EPCs (Figure 2B). Collectively, these results suggested that GAS5 might exert its regulatory function at the post-transcriptional level.

Growth Arrest Specific 5 Promotes Glucose Metabolism Reprogramming and Inhibits Ferroptosis of Endothelial Progenitor Cells Via the IGF2BP1/SIX1 Axis

Growth arrest specific 5 can regulate cellular metabolism, which is closely associated with the fate of EPCs. Thus, the effects of GAS5 on glucose metabolic reprogramming of EPCs were further investigated. As revealed by immunofluorescence staining of 2-NBDG, the glucose uptake of EPCs was significantly suppressed by GAS5 knockdown (Figure 3A). Extracellular acidification rate and OCR are 2 indicators of cell glycolytic capacity. GAS5 silencing was found to reduce ECAR but elevate OCR in EPCs, suggesting that GAS5 regulated the glucose metabolism reprogramming of EPCs (Figure 3B and C). Meanwhile, GAS5 silencing was revealed to induce a significant decrease in glycolysis capacity, ATP level, and elevation in maximal respiration rate (Figure 3D-F). Consistently, glucose uptake testing with 2-DG also indicated that the glucose uptake of EPCs was decreased after silencing GAS5 (Figure 3G). Moreover, the level of lactate (lactic acid) production in GAS5-silenced EPCs was lower relative to the control cells (Figure 3H). Furthermore, GAS5 knockdown also caused the downregulation of PFKL, LDHA, and PKM2 in EPCs (Figure 3I). These results indicate that GAS5 reprograms metabolism

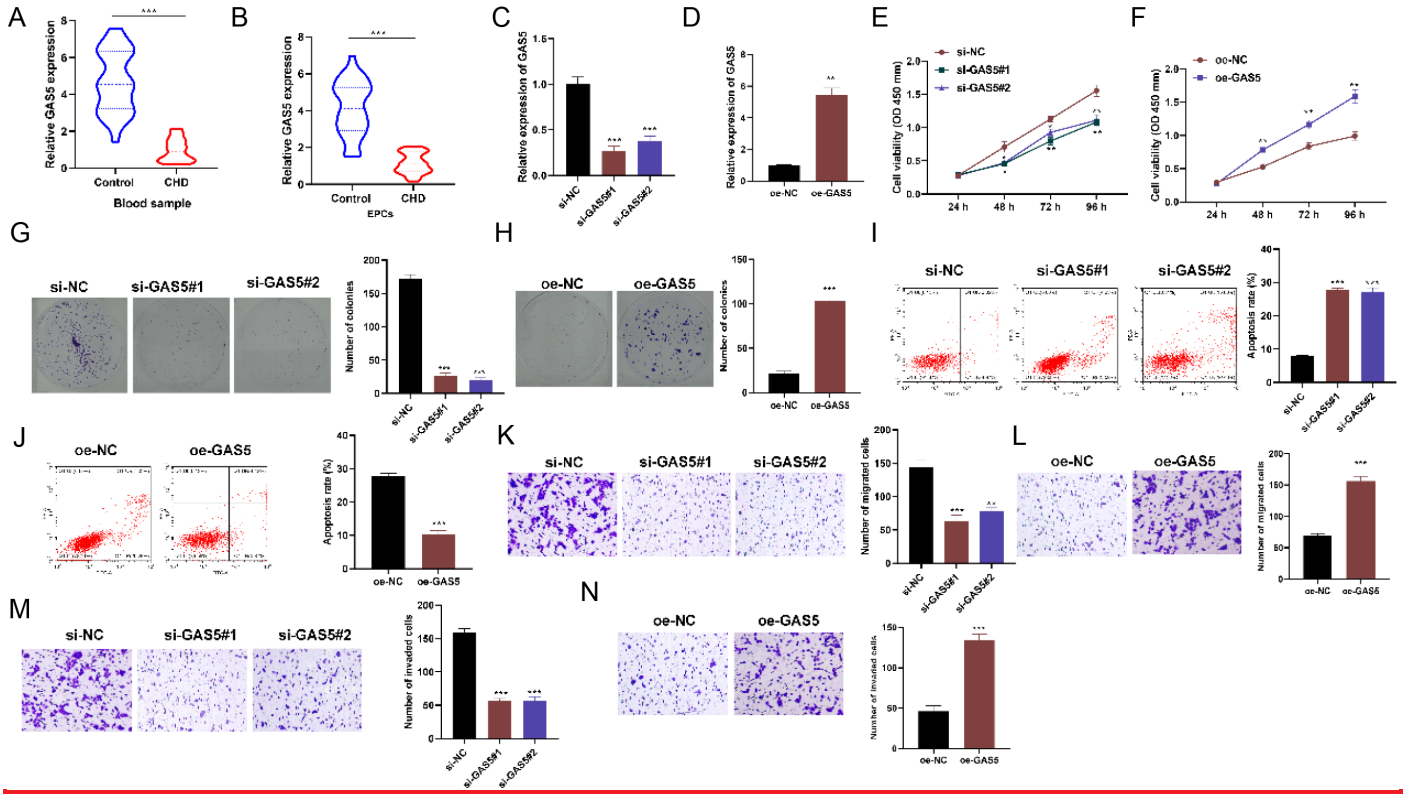

Figure 1. Cell Counting Kit-8 promotes proliferation, migration, and invasion and inhibits apoptosis of EPCs. Reverse transcription-quantitative polymerase chain reaction was used to detect the expression of GAS5 in (A) the blood samples and (B) EPCs collected from healthy individuals (n = 30) and CHD patients (n = 30). Reverse transcription-quantitative polymerase chain reaction detected the efficiency of (C) GAS5 knockdown by si-GAS5#1/2 and (D) overexpression by pcDNA3.1/GAS5 in EPCs. (E-F) Cell Counting Kit-8 assays were conducted to evaluate the viability of EPCs after GAS5 silencing or overexpression. (G, H) Colony formation assays were used to explore the effects of GAS5 silencing or overexpression on the proliferation of EPCs. (I, J) Flow cytometry analysis was used to determine the impact of GAS5 silencing or overexpression on EPC apoptosis. (K-N) Transwell assays were performed to detect the migration and invasion ability of EPCs after GAS5 silencing or overexpression.

to glycolysis. Additionally, GAS5 overexpression is indicated to repress the ferroptosis of hypoxic myocardial cells.[18] For EPCs, GAS5 overexpression significantly reversed the erastin-induced elevation in Fe2+ level, MDA content, and ROS level and reduction in GSH/GSSG level (Figure 3J-M). The evidence indicates that GAS5 suppresses the ferroptosis of EPCs.

Growth Arrest Specific 5 Interacts with IGF2BP1 to Stabilize SIX1

The underlying mechanism of GAS5 to regulate glucose metabolism reprogramming and ferroptosis of EPCs was further investigated. As shown in Supplementary Figure 1A, the regulation of GAS5 on C-Myc, SIX1, and HIF-1 was explored, which are common transcription factors for metabolic

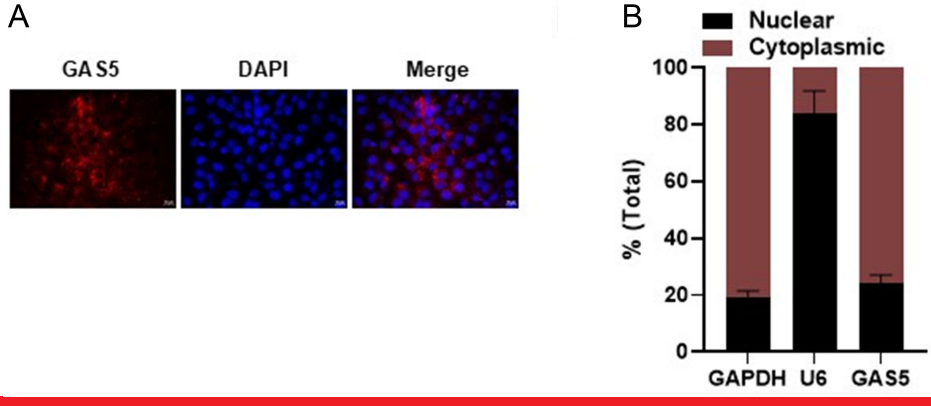

Figure 2. Growth arrest specific 5 is located in the cell cytoplasm and associated with metabolic process. (A) FISH assays and (B) subcellular fractionation assays were performed to detect the subcellular localization of GAS5 in EPCs.

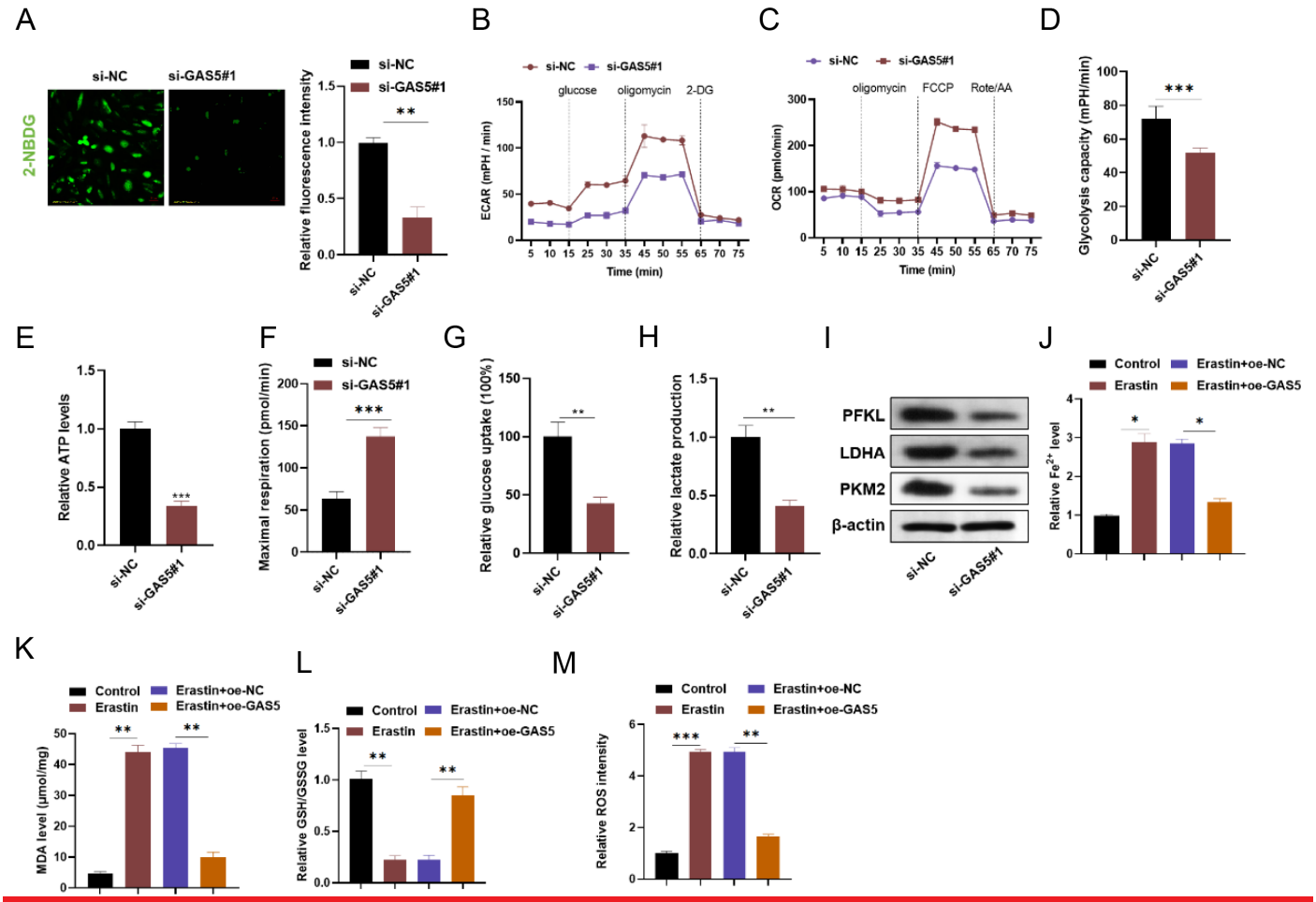

Figure 3. Growth arrest specific 5 promotes glucose metabolic reprogramming and inhibits ferroptosis of EPCs. (A) Immunofluorescence staining of 2-NBDG revealed the glucose uptake of EPCs in the si-NC or si-GAS5#1 group. (B) Extracellular acidification rate and (C) OCR EPCs in the si-NC or si-GAS5#1 group. (D) Glycolysis capacity, (E) ATP level, (F) maximal respiration rate in EPCs in each group. (G) Glucose uptake testing with 2-DG in EPCs. (H) The lactate production in EPCs was measured using commercial kits. (I) Western blot analysis detected the expression of PFKL, LDHA, and PKM2 in EPCs in each group. The effects of GAS5 overexpression on (J) Fe^{2+} level, (K) MDA content, (L) ratio of GSH/GSSG, and (M) ROS level in erastin-treated EPCs.

reprogramming. The results showed that GAS5 knockdown significantly downregulated the expression of SIX1 in EPCs. Thus, the regulation of GAS5 on SIX1 in EPCs was explored. As predicted by the starbase database, IGF2BP1 was an RNA binding protein (RBP) binding to GAS5 and SIX1. RNA pulldown assays verified that IGF2BP1 was enriched in the complex pulled down by Bio-GAS5, which suggested that IGF2BP1 interacted with GAS5 in EPCs (Figure 4A). Meanwhile, RIP assays showed that GAS5 was immunoprecipitated by anti-IGF2BP1 in EPCs, which validated the binding between GAS5 and IGF2BP1 (Figure 4B). Moreover, FISH assays showed that GAS5 and IGF2BP1 were colocalized in the cytoplasm of EPCs (Figure 4C). As IGF2BP1 regulates the stability of various mRNAs, GAS5 was assumed to regulate SIX1 expression via IGF2BP1. Co-immunoprecipitation assays were conducted and showed that IGF2BP1 was immunoprecipitated by anti-SIX1 in EPCs (Figure 4D). Meanwhile, RIP assays revealed that SIX1 was precipitated by anti-IGF2BP1 antibody, while this binding was attenuated by GAS5 knockdown in EPCs, suggesting that GAS5 promoted the binding between IGF2BP1 and SIX1 in EPCs (Figure 4E). The effects of GAS5 silencing and IGF2BP1 overexpression on mRNA stability of SIX1 were evaluated in Actinomycin D (ActD)-treated EPCs. GAS5 knockdown significantly promoted the degradation of SIX1 mRNA, which was reversed by IGF2BP1 overexpression (Figure 4F), suggesting that GAS5 enhanced the mRNA stability of SIX1 via IGF2BP1. Consistently, RT-qPCR analysis revealed that SIX1 expression reduced by GAS5 silencing was partially restored by upregulating IGF2BP1 (Figure 4G). Moreover, the expression levels of SIX1 and GAS5 were positively correlated in blood samples of CHD patients (Figure 4H). Overall, these results indicated that GAS5 binds to IGF2BP1 to enhance the mRNA stability of SIX1.

Growth Arrest Specific 5 Promotes Glucose Metabolism Reprogramming by Upregulating SIX1

Whether SIX1 is involved in GAS5-mediated metabolic reprogramming of EPCs was further explored. SIX1 was overexpressed in EPCs, and the overexpression efficiency was verified by RT-qPCR analysis as well as western blot analysis (Figure 5A). As revealed by CCK-8 assays, SIX1

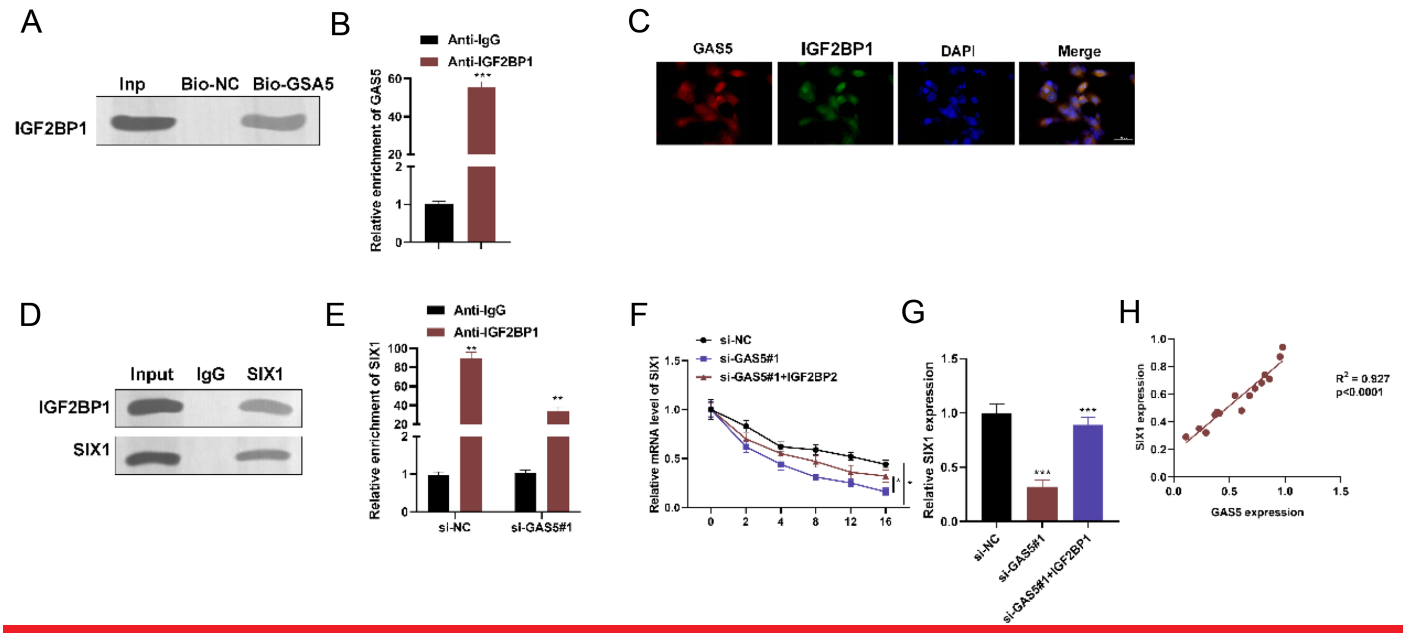

Figure 4. Growth arrest specific 5 interacts with IGF2BP1 to stabilize SIX1. (A) RNA pulldown assay was performed to assess the interaction between IGF2BP1 and GAS5 in EPCs. (B) RNA immunopreciptation (RIP) assays were used to detect the enrichment of GAS5 in the precipitates of anti-IGF2BP1. (C) FISH assays were used to visualize the location of GAS5 and IGF2BP1 in EPCs. (D) Co-immunoprecipitation assays were used to determine the interaction between IGF2BP1 and SIX1 in EPCs. (E) RIP assays were used to determine the impact of GAS5 knockdown on the binding between IGF2BP1 and SIX1. (F) The effects of GAS5 silencing and IGF2BP1 overexpression on the mRNA stability of SIX1 in EPCs treated with ActD. (G) A reverse transcription-quantitative polymerase chain reaction was performed to detect the SIX1 expression in transfected EPCs. (H) The expression correlation between SIX1 and GAS5 in EPCs from CHD patients.

overexpression rescued the inhibition induced by GAS5 deficiency on the viability of EPCs (Figure 5B). The GAS5 silencing-induced reduction in ECAR and elevation in OCR was also significantly restored by SIX1 upregulation (Figure 5C and D). The results of immunofluorescence staining revealed that the glucose uptake of EPCs reduced by GAS5 knockdown was counteracted by overexpressing SIX1 (Figure 5E). Consistently, the GAS5 knockdown-induced reduction in glycolysis capacity, ATP level as well as elevation in maximal respiration rate of EPCs was significantly restored by SIX1 overexpression (Figure 5F-H). Meanwhile, the glucose uptake with 2-DG as well as the lactate production was significantly reduced in response to GAS5 silencing, while SIX1 overexpression reversed this inhibitory effect (Figure 5I and J). Moreover, western blot analysis demonstrated that SIX1 overexpression counteracted the GAS5 deficiency-caused downregulation in protein expression of PFKL, LDHA, and PKM2 in EPCs (Figure 5K). Overall, these results indicate that GAS5 regulates the glucose metabolism reprogramming of EPCs via SIX1.

Growth Arrest Specific 5 Binds to miR-23a-3p to Modulate SLC7A11 Expression

The mechanism of GAS5 to regulate ferroptosis of EPCs was further explored. Substantial literature has revealed that lncRNAs can also function as ceRNAs to regulate gene expression. Based on bioinformatics analysis, the candidate miRNA targets of GAS5 were explored on the ENCORI and lncbase databases. A total of 22 candidate miRNAs were screened by the 2 databases (Supplementary Figure 2A). The level of candidate miRNAs in EPCs from CHD patients and healthy controls was detected using RT-qPCR analysis. Only miR-23a-3p, miR-136-5p and miR-188-5p were found upregulated in the EPCs collected from CHD patients (Supplementary Figure 2B). Furthermore, the RNA pulldown assays showed that only miR-23a-3p was pulled down by bio-GAS5 probes in EPCs, indicating the interaction between miR-23a-3p and GAS5 (Supplementary Figure 2C). Meanwhile, the expression of miR-23a-3p and GAS5 was found to be negatively correlated in the EPCs from CHD patients (Figure 6A). RIP assays showed that GAS5 and miR-23a-3p were abundantly enriched in the precipitates of anti-Ago2, which indicated miR-23a-3p bound to GAS5 in EPCs (Figure 6B). Then miR-23a-3p was overexpressed in EPCs, and the overexpression efficiency was verified using RT-qPCR analysis (Figure 6C). The binding sequence between miR-23a-3p and GAS5 was predicted by the Encyclopedia of RNA Interactomes (ENCORI) database, and Wt or Mut luciferase reporter vector was constructed for assessing the interaction between miR-23a-3p and GAS5. The results demonstrated that miR-23a-3p overexpression induced the reduction in luciferase reporter activity of GAS5-wt luciferase reporter vector while showed no significant influence on the Mut group, suggesting that GAS5 bound to miR-23a-3p (Figure 6D and E). Meanwhile, RT-qPCR analysis showed evident upregulation of miR-23a-3p in GAS5-silenced EPCs (Figure 6F). Moreover, the downstream targets of miR-23a-3p was further investigated. MiR-23a-3p has also been revealed to promote the ferroptosis of cardiomyocytes by targeting ferroptosis mediator SLC7A11.[19] Based

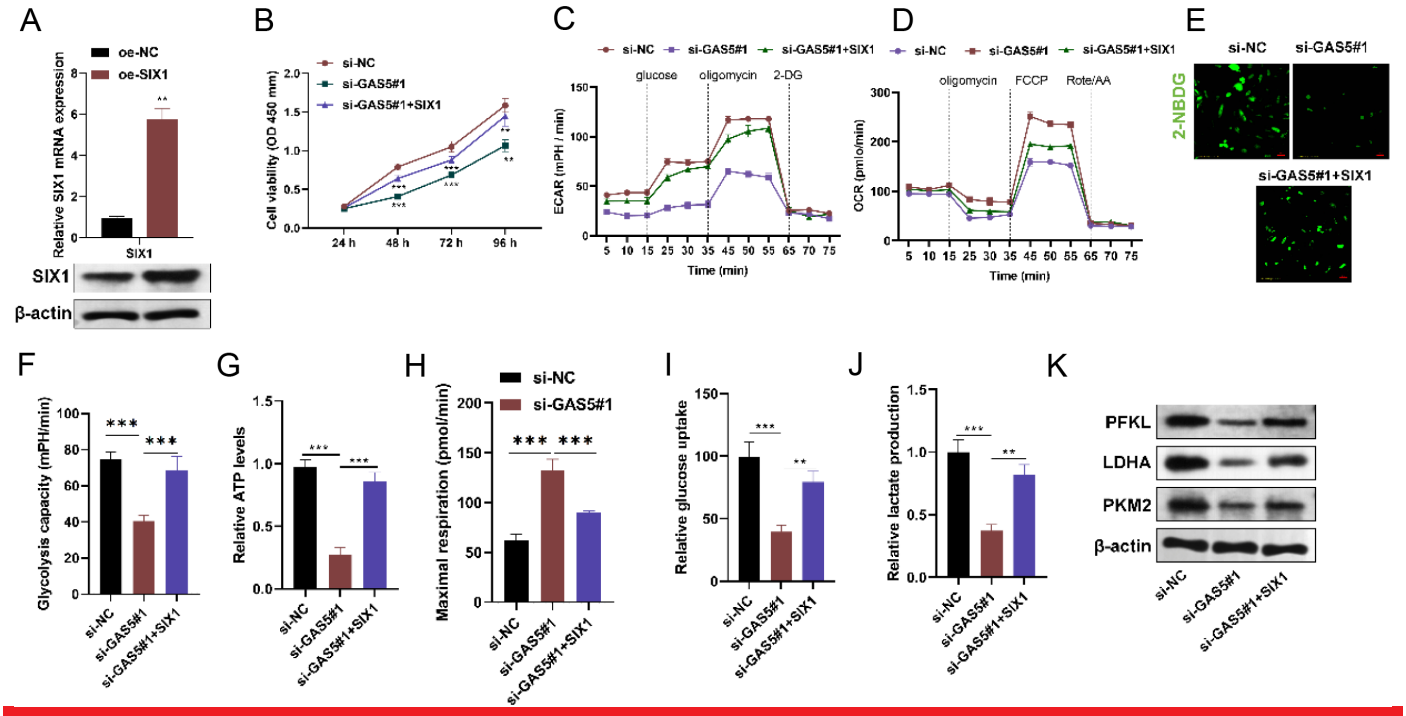

Figure 5. Growth arrest specific 5 promotes glucose metabolism reprogramming by upregulating SIX1. (A) Reverse transcription-quantitative polymerase chain reaction and western blot detected the expression of SIX1 in EPCs transfected with oe-NC or oe-SIX1. (B) Cell Counting Kit-8 assays were used to determine the viability of EPCs in each group. (C) Extracellular acidification rate and (D) OCR of transfected EPCs. (E) Immunofluorescence staining of 2-NBDG showed the glucose uptake of EPCs in each group. (F) Glycolysis capacity, (G) ATP level, (H) maximal respiration rate of EPCs. (I) glucose uptake with 2-DG in EPCs. (J) Lactate production in ECPs. (K) Western blot analysis was used to detect the protein expression of PFKL, LDHA, and PKM2 in EPCs in each group.

on Pearson correlation analysis, the level of miR-23a-3p was found to be negatively correlated with SLC7A11 level in EPCs from CHD patients (Figure 6G). Furthermore, RNA pulldown assays demonstrated the enrichment of SLC7A11 in the RNA complexes pulled down by the bio-miR-23a-3p probe in EPCs (Figure 6H). Consistently, miR-23a-3p overexpression decreased the luciferase reporter activities in the wt group while not significantly altering those in the Mut group, suggesting that miR-23a-3p targeted SLC7A11 in EPCs (Figure 6I and J). Additionally, miR-23a-3p overexpression also caused a significant downregulation of SLC7A11 mRNA and protein levels in EPCs (Figure 6K). Then whether GAS5 regulated the miR-23a-3p/SLC7A11 axis in EPCs was investigated. The expression of GAS5 and SLC7A11 was in positive correlation in the EPCs from CHD patients (Figure 6L). SLC7A11 mRNA and protein expression also showed a significant decrease in GAS5-silenced EPCs (Figure 6M). Importantly, GAS5 overexpression induced an upregulation of SLC7A11 mRNA and protein, which was significantly reversed by overexpressing miR-23a-3p (Figure 6N and O). Overall, GAS5 binds to miR-23a-3p to upregulate SLC7A11 in EPCs.

Growth Arrest Specific 5 Inhibits Ferroptosis of Endothelial Progenitor Cells Via SLC7A11

Further investigation was conducted on whether SLC7A11 was involved in GAS5-mediated ferroptosis of EPCs. The viability of EPCs reduced in response to erastin treatment was reversed after GAS5 overexpression, while SLC7A11 silencing attenuated the protective effects of GAS5 on EPCs, as evidenced by the reduced viability of EPCs (Figure 7A). The Fe^{2+} level and MDA content increased by erastin treatment was reversed by GAS5 overexpression and showed a significant increase by silencing SLC7A11 (Figure 7B and C). Growth arrest specific 5 overexpression also restored the erastin-caused reduction in GSH/GSSG ratio and elevation in elevation in ROS level, which was both counteracted by silencing SLC7A11 in EPCs (Figure 7D and E). Additionally, the lactate dehydrogenase (LDH) release elevated by erastin was reduced by overexpressing GAS5 and showed significant elevation after the co-transfection of si-SLC7A11 (Figure 7F). Moreover, the levels of ferroptosis-related markers were detected using western blot. The erastin-caused downregulation of SLC7A11 and GPX4, as well as upregulation of ACSL4, was reversed by overexpressing GAS5, while the co-transfection of SLC7A11 showed counteractive effects, as evidenced by significantly decreased SLC7A11 and GPX4 expression and increased ACSL4 level in EPCs (Figure 7G). Overall, these findings suggest that GAS5 inhibits the ferroptosis of EPCs by upregulating SLC7A11.

DISCUSSION

Cardiovascular diseases remain a major cause of death globally, taking nearly 18 million lives annually, among which CHD is responsible for an estimated 7.4 million death cases.[20] However, the therapeutic interventions for CHD are still

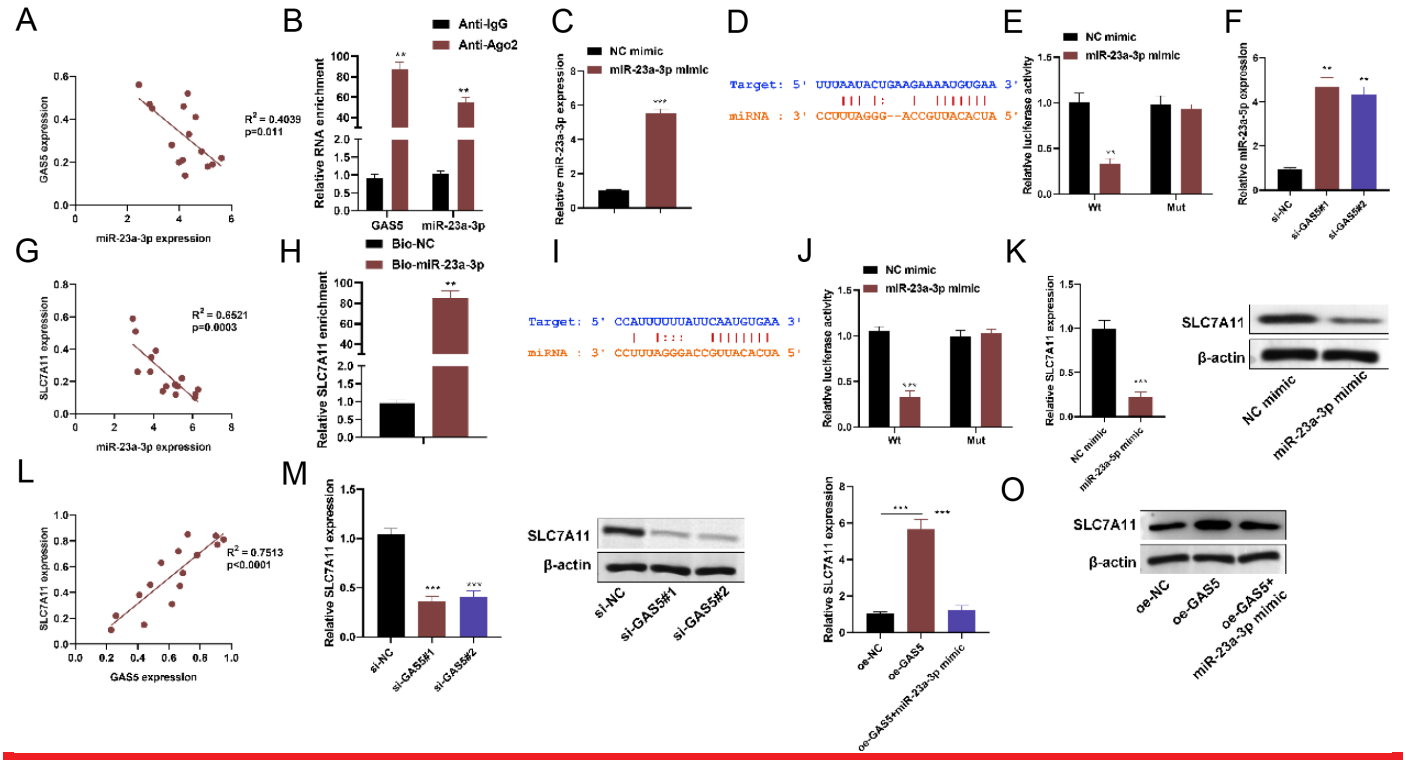

Figure 6. Growth arrest specific 5 interacts with miR-23a-3p to regulate SLC7A11. (A) The expression correlation between GAS5 and miR-23a-3p in EPCs from CHD patients. (B) RIP assays were used to determine the interaction between GAS5 and miR-23a-3p in EPCs. (C) Reverse transcription-quantitative polymerase chain reaction was used to detect the overexpression efficiency of miR-23a-3p in EPCs. (D) The binding sequence between GAS5 and miR-23a-3p was predicted on the ENCORI database. (E) Luciferase reporter assays were used to assess the binding between miR-23a-3p and GAS5 in EPCs. (F) Reverse transcription-quantitative polymerase chain reaction detected the miR-23a-3p expression in EPCs after GAS5 knockdown. (G) The expression correlation between miR-23a-3p and SLC7A11 in EPCs from CHD patients. (H) RNA pulldown assays were used to detect the interaction between miR-23a-3p and SLC7A11 in EPCs. (I) The binding sequence between miR-23a-3p and SLC7A11 was predicted on the ENCORI database. (J) Luciferase reporter assays were used to determine the binding between miR-23a-3p and SLC7A11 in EPCs. (K) Reverse transcription-quantitative polymerase chain reaction and western blot analyses were used to detect the expression of SLC7A11 in EPCs after miR-23a-3p overexpression. (L) The expression correlation between SLC7A11 and GAS5 in EPCs from CHD patients. (M) Reverse transcription-quantitative polymerase chain reaction and western blot analyses were used to detect the expression of SLC7A11 in EPCs after GAS5 knockdown. (N-O) Reverse transcription-quantitative polymerase chain reaction and western blot analyses were used to detect the expression of SLC7A11 in EPCs after GAS5 and miR-23a-3p overexpression.

limited, and patients suffer from complications with unfavorable outcomes. Thus, it is essential to explore effective therapeutic targets to improve the treatment of CHD.

LncRNAs are closely associated with the progression of cardiovascular diseases by regulating diverse biological processes including inflammation, cell proliferation, apoptosis, as well as senescence.[21] Functionally, lncRNAs are known as regulators for mRNA decay or sponging miRNAs to prevent the inhibitory effects of miRNAs on the stability or the translation of their targets at post-transcriptional levels.[22,23] Amount of research has shown that GAS5 regulates the proliferation, migration, invasion as well as apoptosis of tumor cells.[24-26] In cardiovascular diseases, GAS5 is indicated to play diverse roles. For example, some studies have shown that GAS5 knockdown shows protective effects against high glucose-induced cardiomyocyte damage, myocardial ischemia/reperfusion injury, as well as myocardial infarction-induced cardiomyocyte apoptosis.[27-29] However, there are also some studies that reveal that GAS5 alleviates endothelial cell injury in cardiovascular diseases. For example, GAS5 overexpression enhances the proliferation, migration, and angiogenesis abilities of cardiac microvascular endothelial cells and inhibits cell apoptosis.[30] Additionally, a study has revealed that GAS5 knockdown suppresses EPC proliferation and facilitates EPC senescence.[14] Thus, GAS5 can also play cardioprotective roles by modulating the function of EPCs. This study revealed that GSA5 was downregulated in the blood sample and EPCs in CHD patients compared with healthy individuals. The effects of GSA5 on the function of EPCs were further investigated.

In recent decades, the potential of endothelial progenitor cells has been noticed in the treatment of cardiovascular diseases. As a group of cells released from bone marrow into peripheral blood, EPCs effectively promote endothelial repair and neovasculogenesis, and are thus considered useful for the cell therapy of ischemic heart disease.[31] Clinical

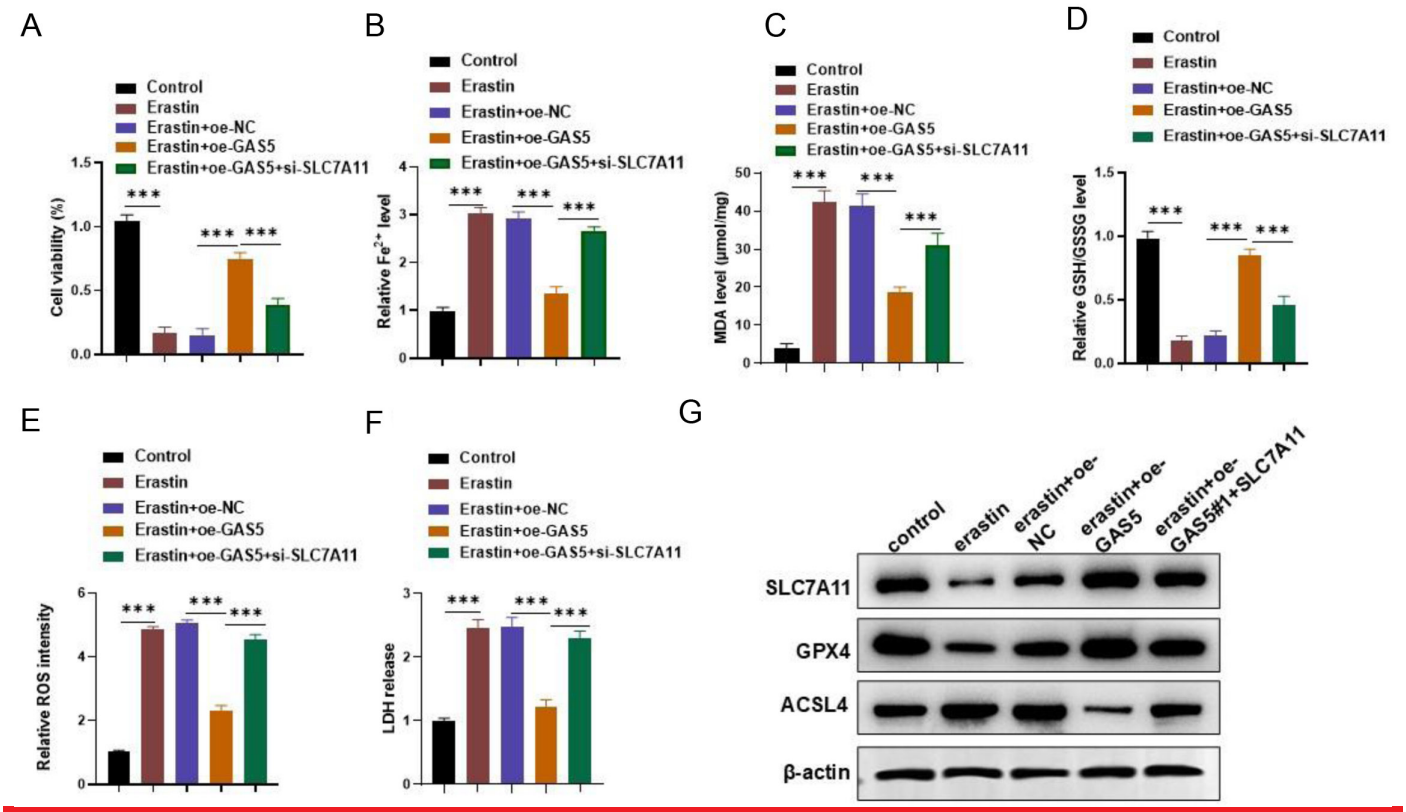

Figure 7. Growth arrest specific 5 inhibits EPC ferroptosis by upregulating SLC7A11. (A) Cell Counting Kit-8 assays were used to detect the viability of EPCs in each group. (B) Fe^{2+} level, (C) MDA content, (D) GSH/GSSG ratio, (E) ROS level, and (F) LDH release in each group of EPCs. (G) Western blot detected the levels of ferroptosis-related markers in EPCs.

studies have revealed that the proliferation, and migration abilities of EPCs are impaired and the apoptosis rate is elevated in acute coronary syndrome patients.[32,33] Moreover, restoring EPC function has been revealed to show protective effects against cardiovascular diseases. For example, miR-214 regulates EPC vasculogenesis and migration by targeting vascular endothelial growth factor (VEGF) in CHD.[34] G-protein-coupled receptor 4 (GPR4) overexpression promotes the neovessel formation of EPCs from patients with coronary artery disease by activating the STAT3/VEGFA pathway.[35] Sirtuin 1 alleviates mouse coronary atherosclerosis by facilitating EPC proliferation and migration.[36] In our work, GAS5 silencing represses the proliferative capacity, migration, and invasion ability, and elevates the apoptotic rate of EPCs. Growth arrest specific 5 overexpression was demonstrated to facilitate EPC growth, migration, invasion and suppress apoptosis, suggesting the beneficial effects of GAS5 by improving the function of EPCs against CHD.

Glucose metabolic reprogramming is induced by myocardial infarction. However, the changes cannot support cardiomyocyte proliferation to replace lost cells caused by the ischemic injury.[37] Metabolic reprogramming is indicated to promote cardiac regeneration following injury, while the underlying targets need further investigation. Wang et al[38] have found that PPARγ agonist promotes cardiac glucose metabolic reprogramming by enhancing glycolytic capacity and reducing mitochondrial reactive ROS production via HIF-1α to prevent hypoxia-induced cardiac dysfunction. A study reveals that VEGF-B reprograms myocardial metabolism to enhance cardiac function in ischemic heart disease.[39] In our study, GAS5 silencing was demonstrated to inhibit glucose metabolic reprogramming by reducing glycolysis capacity, glucose uptake, and lactate production. SIX1 is a critical transcription regulator of glycolysis. In our previous study, GAS5 was found to regulate glucose metabolism reprogramming of EPCs via the miR-495-3p/SIX1 and IGF2BP2/NRF2 dual-regulatory pathways.[16] In this study, GAS5 was further found to directly bind to IGF2BP1 to enhance the mRNA stability of SIX1 in EPCs. Moreover, rescue assays proved that GAS5 promoted the glucose metabolic reprogramming of EPCs by upregulating SIX1.

Ferroptosis is a novel form of iron-dependent programmed cell death. Studies have shown that anti-ferroptosis strategies can alleviate cell injury in coronary heart disease. For example, SGK1 deficiency attenuates the erastin-caused ferroptosis of mouse aortic endothelial cells by reversing the erastin-caused decrease in SLC7A11, GPX4, and GSH/GSSG and elevation in lipid peroxidation as well as Fe accumulation.[40] SLC7A11 as an amino acid transporter plays a crucial role in regulating GSH synthesis and cellular ferroptosis. In our previous study, GAS5 was found to participate in the progression of CHD by regulating ferroptosis of EPCs through the miR-495-3p/SIX1 and IGF2BP2/NRF2 dual-regulatory pathways.[16] The current study has confirmed for the first

time that GAS5 can interact with miR-23a-3p to upregulate SLC7A11, thereby protecting EPCs from ferroptosis in CHD.

CONCLUSION

Growth arrest specific 5 is downregulated in EPCs collected from CHD patients, and overexpression of GAS5 promotes glucose metabolism reprogramming via the IGF2BP1/SIX1 axis and inhibits ferroptosis of EPCs via the miR-23a-3p/SLC7A11 axis. The findings of our study might provide novel therapeutic targets for EPC protection in CHD treatment.

Data Availability Statement: The datasets generated during and/or analyzed during the current study are available from the corresponding author upon reasonable request.

Ethics Committee Approval: This study was approved by the Ethics Committee of Zhujiang Hospital, Southern Medical University. The procedures used in this study adhere to the tenets of the Declaration of Helsinki.

Informed Consent: All participants had signed the informed consent.

Peer-review: Internally peer-reviewed.

Author Contributions: Conception – M.Z.; Design – M.Z., W.X., B.T.; Supervision – M.Z., Y.L.; Materials – W.X., B.T., Y.L.; Data Collection and/or Processing – W.X., B.T., Q.Z., Z.J.; Analysis and/or Interpretation – M.Z., Q.Z., Z.J.; Literature Review – Q.Z., Z.J.; Writing – M.Z.; Critical Review – Y.L. All authors read and approved the final manuscript.

Declaration of Interests: The authors have no conflicts of interest to declare.

Funding: The authors declare that this study received no financial support.

REFERENCES

1. Wang Z, Ma L, Liu M, Fan J, Hu S, Writing Committee of the Report on Cardiovascular Health and Diseases in China. Summary of the 2022 report on cardiovascular health and diseases in china. *Chin Med J (Engl)*. 2023;136(24):2899-2908. [CrossRef]
2. Chepeleva EV. Cell therapy in the treatment of coronary heart disease. *Int J Mol Sci*. 2023;24(23):16844. [CrossRef]
3. Matsuzawa Y, Guddeti RR, Kwon TG, Lerman LO, Lerman A. Treating coronary disease and the impact of endothelial dysfunction. *Prog Cardiovasc Dis*. 2015;57(5):431-442. [CrossRef]
4. Morrone D, Picoi MEL, Felice F, et al. Endothelial progenitor cells: an appraisal of relevant data from bench to bedside. *Int J Mol Sci*. 2021;22(23):12874. [CrossRef]
5. Hu Z, Wang H, Fan G, et al. Danhong injection mobilizes endothelial progenitor cells to repair vascular endothelium injury via upregulating the expression of Akt, eNOS and MMP-9. *Phytomedicine*. 2019;61:152850. [CrossRef]
6. Vasa M, Fichtlscherer S, Adler K, et al. Increase in circulating endothelial progenitor cells by statin therapy in patients with stable coronary artery disease. *Circulation*. 2001;103(24):2885-2890. [CrossRef]
7. Yan F, Li J, Zhang W. Transplantation of Endothelial Progenitor Cells: summary and prospect. *Acta Histochem*. 2023;125(1):151990. [CrossRef]
8. Kopp F, Mendell JT. Functional classification and experimental dissection of long noncoding RNAs. *Cell*. 2018;172(3):393-407. [CrossRef]
9. Rinn JL, Chang HY. Long noncoding RNAs: molecular modalities to organismal functions. *Annu Rev Biochem*. 2020;89:283-308. [CrossRef]
10. Yao RW, Wang Y, Chen LL. Cellular functions of long noncoding RNAs. *Nat Cell Biol*.2019;21(5):542-551. [CrossRef]
11. Li P, Li Y, Chen L, et al. Long noncoding RNA uc003pxg.1 regulates endothelial cell proliferation and migration via miR255p in coronary artery disease. *Int J Mol Med*. 2021;48(2).
12. Zhang H, Ji N, Gong X, Ni S, Wang Y. NEAT1/miR-140-3p/MAPK1 mediates the viability and survival of coronary endothelial cells and affects coronary atherosclerotic heart disease. *Acta Biochim Biophys Sin (Shanghai)*. 2020;52(9):967-974. [CrossRef]
13. Hao S, Liu X, Sui X, Pei Y, Liang Z, Zhou N. Long non-coding RNA GAS5 reduces cardiomyocyte apoptosis induced by MI through sema3a. *Int J Biol Macromol*. 2018;120(Pt A):371-377. [CrossRef]
14. Yao J, Shi Z, Ma X, Xu D, Ming G. lncRNA GAS5/miR-223/NAMPT axis modulates the cell proliferation and senescence of endothelial progenitor cells through PI3K/AKT signaling. *J Cell Biochem*. 2019;120(9):14518-14530. [CrossRef]
15. Chen T, Liang Q, Xu J, et al. MiR-665 regulates vascular smooth muscle cell senescence by interacting with LncRNA GAS5/SDC1. *Front Cell Dev Biol*. 2021;9:700006. [CrossRef]
16. Zhong M, Xu W, Tang B, Zhao Q, Jiang Z, Liu Y. GAS5 promotes glucose metabolism reprogramming and resistance to ferroptosis of endothelial progenitor cells through the miR-495-3p/SIX1 and IGF2BP2/NRF2 dual-regulatory pathways in coronary heart disease. *Cell Mol Biol (Noisy-Le-Grand)*. 2024;70(9):121-128. [CrossRef]
17. Ikutomi M, Sahara M, Nakajima T, et al. Diverse contribution of bone marrow-derived late-outgrowth endothelial progenitor cells to vascular repair under pulmonary arterial hypertension and arterial neointimal formation. *J Mol Cell Cardiol*. 2015;86:121-135. [CrossRef]
18. Ren Y, Zhao X. Bone marrow mesenchymal stem cells-derived exosomal lncRNA GAS5 mitigates heart failure by inhibiting UL3/Hippo pathway-mediated ferroptosis. *Eur J Med Res*. 2024;29(1):303. [CrossRef]
19. Liu D, Yang M, Yao Y, et al. Cardiac fibroblasts promote ferroptosis in atrial fibrillation by secreting Exo-miR-23a-3p targeting SLC7A11. *Oxid Med Cell Longev*. 2022;2022:3961495. [CrossRef]
20. Organization WH. *Fact Sheet on Cardiovascular Disease*. World Health Organization. 2013. [CrossRef]
21. Yeh CF, Chang YE, Lu CY, Hsuan CF, Chang WT, Yang KC. Expedition to the missing link: long noncoding RNAs in cardiovascular diseases. *J Biomed Sci*. 2020;27(1):48. [CrossRef]
22. Zhang L, Yang Z, Trottier J, Barbier O, Wang L. Long noncoding RNA MEG3 induces cholestatic liver injury by interaction with PTBP1 to facilitate shp mRNA decay. *Hepatology*. 2017;65(2):604-615. [CrossRef]
23. Tay Y, Rinn J, Pandolfi PP. The multilayered complexity of ceRNA crosstalk and competition. *Nature*. 2014;505(7483):344-352. [CrossRef]
24. Ni W, Yao S, Zhou Y, et al. Long noncoding RNA GAS5 inhibits progression of colorectal cancer by interacting with and triggering YAP phosphorylation and degradation and is negatively regulated by the m(6)A reader YTHDF3. *Mol Cancer*. 2019;18(1):143. [CrossRef]
25. Zhang Z, Liu T, Cheng C, et al. LncRNA GAS5 regulates the Wnt/β-catenin pathway through the miR-18a-5p/AXIN2/GSK3β axis to inhibit the proliferation and migration of bladder cancer cells. *Carcinogenesis*. 2022;43(12):1176-1189. [CrossRef]

26. Zhu L, Zhou D, Guo T, et al. LncRNA GAS5 inhibits Invasion and Migration of Lung Cancer through influencing EMT process. *J Cancer*. 2021;12(11):3291-3298. [CrossRef]
27. Zhou XH, Chai HX, Bai M, Zhang Z. LncRNA-GAS5 regulates PDCD4 expression and mediates myocardial infarction-induced cardiomyocytes apoptosis via targeting MiR-21. *Cell Cycle*. 2020;19(11):1363-1377. [CrossRef]
28. Wu N, Zhang X, Bao Y, Yu H, Jia D, Ma C. Down-regulation of GAS5 ameliorates myocardial ischaemia/reperfusion injury via the miR-335/ROCK1/AKT/GSK-3β axis. *J Cell Mol Med*. 2019;23(12):8420-8431. [CrossRef]
29. Zhuo X, Bai K, Wang Y, et al. Long-chain noncoding RNA-GAS5/hsa-miR-138-5p attenuates high glucose-induced cardiomyocyte damage by targeting CYP11B2. *Biosci Rep*. 2021;41(9):BSR20202232. [CrossRef]
30. Diao L, Bai L, Jiang X, Li J, Zhang Q. Long-chain noncoding RNA GAS5 mediates oxidative stress in cardiac microvascular endothelial cells injury. *J Cell Physiol*. 2019;234(10):17649-17662. [CrossRef]
31. Bianconi V, Sahebkar A, Kovanen P, et al. Endothelial and cardiac progenitor cells for cardiovascular repair: a controversial paradigm in cell therapy. *Pharmacol Ther*. 2018;181:156-168. [CrossRef]
32. Zhang LJ, Liu WX, Chen YD, Song XT, Jin ZN, Lü SZ. Proliferation, migration and apoptosis activities of endothelial progenitor cells in acute coronary syndrome. *Chin Med J (Engl)*. 2010;123(19):2655-2661.
33. Solomon A, Blum A, Peleg A, Lev EI, Leshem-Lev D, Hasin Y. Endothelial progenitor cells are suppressed in anemic patients with acute coronary syndrome. *Am J Med*. 2012;125(6):604-611. [CrossRef]
34. Jin Y, Yang CJ, Xu X, Cao JN, Feng QT, Yang J. MiR-214 regulates the pathogenesis of patients with coronary artery disease by targeting VEGF. *Mol Cell Biochem*. 2015;402(1-2):111-122. [CrossRef]
35. Ouyang S, Li Y, Wu X, et al. GPR4 signaling is essential for the promotion of acid-mediated angiogenic capacity of endothelial progenitor cells by activating STAT3/VEGFA pathway in patients with coronary artery disease. *Stem Cell Res Ther*. 2021;12(1):149. [CrossRef]
36. Li Y, Cui W, Song B, Ye X, Li Z, Lu C. Autophagy-sirtuin1(SIRT1) alleviated the coronary atherosclerosis (AS)in mice through regulating the proliferation and migration of endothelial progenitor cells (EPCs) via wnt/β-catenin/GSK3β signaling pathway. *J Nutr Health Aging*. 2022;26(3):297-306. [CrossRef]
37. Chen X, Wu H, Liu Y, Liu L, Houser SR, Wang WE. Metabolic reprogramming: a byproduct or a driver of cardiomyocyte proliferation? *Circulation*. 2024;149(20):1598-1610. [CrossRef]
38. Wang Y, Zhang R, Chen Q, et al. PPARγ agonist pioglitazone prevents hypoxia-induced cardiac dysfunction by reprogramming glucose metabolism. *Int J Biol Sci*. 2024;20(11):4297-4313. [CrossRef]
39. Kivelä R, Bry M, Robciuc MR, et al. VEGF-B-induced vascular growth leads to metabolic reprogramming and ischemia resistance in the heart. *EMBO Mol Med*. 2014;6(3):307-321. [CrossRef]
40. Peng Y, Jiang Y, Zhou Q, Jia Z, Tang H. SGK1 contributes to ferroptosis in coronary heart disease through the NEDD4L/NF-κB pathway. *J Mol Cell Cardiol*. 2024;196:71-83. [CrossRef]

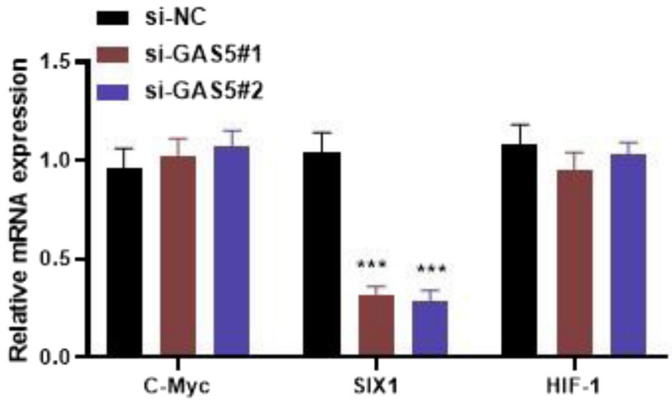

Supplementary Figure 1. Regulation of GAS5 on ferroptosis-related transcription factors. (A) RT-qPCR was used to detect the expression of ferroptosis-related transcription factors including C-myc, SIX1 and HIF-1 in EPCs after GAS5 knockdown.

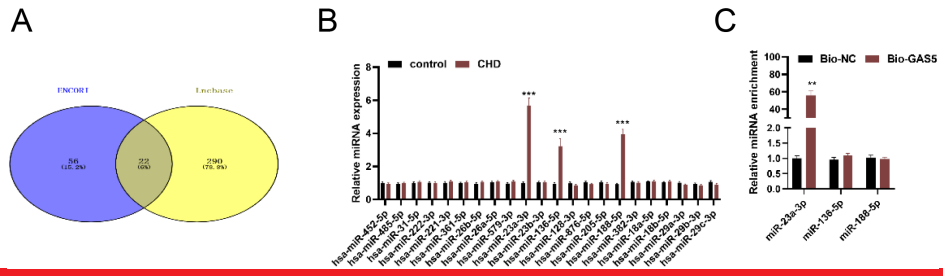

Supplementary Figure 2. MiR-23a-3p was targeted by GAS5. (A) The venn diagram showed shared miRNA targets of GAST in ENCORI database and lncbase database. (B) RT-qPCR was used to measure the expression of candidate miRNAs in control and CHD group. (C) RNA pulldown assays were used to evaluate the binding between miRNAs with GAS5 in EPCs.

Supplementary Table 1. Specific experimental data of Figure 1A-B

Indicators	Control (n=30)	CHD (n=30)	*P* value
GAS5 in blood samples	0.98 ± 0.61	4.67 ± 1.66	<0.001
GAS5 in EPCs	1.13 ± 0.56	4.13 ± 1.48	<0.001

Supplementary Table 2. Specific experimental data of Figure 1C, 1E, 1G, 1I, 1K, and 1M , E, G, I, K, M)

Indicators	si-NC (n=3)	si-GAS5#1 (n=3)	si-GAS5#2 (n=3)	*P* value (si-GAS5#1 vs. si-NC)	*P* value (si-GAS5#2 vs. si-NC)
GAS5	1 ± 0.08	0.27 ± 0.06	0.38 ± 0.06	<0.001	<0.001
Cell viability				<0.001	<0.001
24 h	0.28 ± 0.02	0.29 ± 0.02	0.28 ± 0.03	>0.999	>0.999
48 h	0.71 ± 0.08	0.46 ± 0.04	0.47 ± 0.05	0.033	0.035
72 h	1.13 ± 0.04	0.80 ± 0.06	0.93 ± 0.05	0.003	0.013
96 h	1.56 ± 0.09	1.08 ± 0.05	1.11 ± 0.08	0.006	0.006
Number of colonies	171.3 ± 7.02	26.67 ± 4.16	20.33 ± 3.22	<0.001	<0.001
Apoptosis rates (%)	7.93 ± 0.23	27.65 ± 0.74	27.29 ± 1.12	<0.001	<0.001
Number of migrated cells	144.3 ± 11.06	62.67 ± 9.29	78.67 ± 4.51	<0.001	0.004
Number of invaded cells	158.7 ± 6.43	56.67 ± 3.51	56.33 ± 6.66	<0.001	<0.001

Supplementary Table 3. Specific experimental data of Figure 1D, 1F, 1H, 1J, 1L, and 1N

Indicators	oe-NC (n=3)	oe-GAS5 (n=3)	*P* value
GAS5	0.96 ± 0.07	5.43 ± 0.45	0.003
Cell viability			
24 h	0.30 ± 0.02	0.27 ± 0.03	0.286
48 h	0.53 ± 0.04	0.78 ± 0.04	0.001
72 h	0.84 ± 0.05	1.16 ± 0.07	0.003
96 h	0.99 ± 0.06	1.59 ± 0.10	0.002
Number of colonies	21.67 ± 2.52	103.3 ± 6.11	<0.001
Apoptosis rates (%)	27.73 ± 0.96	10.32 ± 1.12	<0.001
Number of migrated cells	69 ± 3.61	156.3±7.51	<0.001
Number of invaded cells	46.33 ± 6.81	134.7 ± 7.02	<0.001

Supplementary Table 4. Specific experimental data of Figure 2B

Indicators	Nuclear (n=3)	Cytoplasmic (n=3)	*P* value
GAS5	23.6 ± 3.2	76.4 ± 6.5	0.001
GAPDH	19.1 ± 2.5	80.9 ± 7.3	0.002
U6	84.2 ± 7.4	15.8 ± 2.2	0.002

Supplementary Table 5. Specific experimental data of Figure 3A-H

Indicators	si-NC (n=3)	si-GAS5#1 (n=3)	*P* value
Relative fluorescence intensity	1 ± 0.05	0.33 ± 0.10	0.002
ECAR			
5	39.67 ± 1.53	20 ± 1	<0.001
10	40.67 ± 2.08	18 ± 1	<0.001
15	34.67 ± 1.53	17.33 ± 1.53	<0.001
25	60.33 ± 3.22	27 ± 2	<0.001
30	60 ± 2	27 ± 3.61	<0.001
35	64.67 ± 5.51	32 ± 3	0.003
45	113 ± 12.29	70.67 ± 3.06	0.02
50	109.3 ± 2.52	68.33 ± 3.22	<0.001
55	108.3 ± 4.93	71.67 ± 3.06	0.001
65	27.67 ± 2.52	20.67 ± 2.52	0.027
70	24.33 ± 1.53	22 ± 2	0.189
75	22 ± 1	18.33 ± 2.08	0.074
OCR			
5	85.67 ± 4.04	105.7 ± 6.03	0.01
10	91.33 ± 3.06	105 ± 7.94	0.082
15	88.67 ± 2.52	100 ± 5.29	0.047
25	52.33 ± 6.43	81.33 ± 6.81	0.006
30	54.67 ± 3.06	80.33 ± 3.22	<0.001
35	56 ± 3	82.33 ± 2.52	<0.001
45	156.3 ± 7.37	251.7 ± 8.02	<0.001
50	151.3 ± 4.04	236.3 ± 6.11	<0.001
55	148 ± 5.57	234.7 ± 6.11	<0.001
65	36 ± 2	49 ± 3	0.005
70	39 ± 3	53 ± 2.65	0.004
75	37.33 ± 2.52	48.67 ± 2.52	0.005
Glycolysis capacity	71.89 ±7.61	51.78 ± 2.91	<0.001
Relative ATP levels	1.0 ± 0.06	0.34 ± 0.04	<0.001
Maximal respiration	63.33 ± 8.44	137.3 ± 10.56	<0.001
Relative glucose uptake	100.2 ± 12.4	42.5 ± 5.7	0.007
Relative lactate production	1.0 ± 0.1	0.41 ± 0.05	0.003

Supplementary Table 6. Specific experimental data of Figure 3J-M

Indicators	Control (n=3)	Erastin (n=3)	Erastin+oe-NC (n=3)	Erastin+oe-GAS5 (n=3)	*P* value (Erastin vs. Control)	*P* value (Erastin+oe-GAS5 vs. Erastin+oe-NC)
Relative Fe 2+ level	0.99 ± 0.04	2.88 ± 0.23	2.86 ± 0.11	1.33 ± 0.10	0.017	0.014
MDA level	4.6 ± 0.72	44.07 ± 2.17	45.37 ± 1.44	9.9 ± 1.7	0.004	0.003
Relative GSH/GSSG level	1.01 ± 0.07	0.23 ± 0.04	0.23 ± 0.04	0.85 ± 0.08	0.01	0.004
Relative ROS intensity	1.0 ± 0.08	4.95 ± 0.09	4.95 ± 0.15	1.65 ± 0.09	<0.001	0.002

Supplementary Table 7. Specific experimental data of Figure 4B and 4E

Indicators	Anti-IgG (n=3)	Anti-IGF2BP1 (n=3)	*P* value
Relative enrichment of GAS5	1.0 ± 0.09	55.3 ± 3.16	0.001
Relative enrichment of SIX1			
si-NC	0.98 ± 0.08	89.43 ± 6.72	0.002
si-GAS5#1	1.02 ± 0.09	34.2 ± 4.2	0.005

Supplementary Table 8. Specific experimental data of Figure 4F-G

Indicators	si-NC (n=3)	si-GAS5#1 (n=3)	si-GAS5#1+IGF2BP1 (n=3)	*P* value (si-GAS5#1 vs. si-NC)	*P* value (si-GAS5#1+IGF2BP1 vs. si-GAS5#1)
Relative mRNA level of SIX1					
0	1.0 ± 0.1	1.0 ± 0.08	1.0 ± 0.07	>0.999	>0.999
2	0.83± 0.06	0.62± 0.06	0.70± 0.06	0.012	0.304
4	0.62± 0.05	0.44 ± 0.06	0.55 ± 0.05	0.015	0.1
8	0.59± 0.05	0.31 ± 0.03	0.47 ± 0.06	0.001	0.016
12	0.52 ± 0.04	0.25 ± 0.04	0.36 ± 0.07	0.002	0.091
16	0.44± 0.04	0.16 ± 0.04	0.32 ± 0.06	0.001	0.015
Relative SIX1 expression	1.0 ± 0.08	0.32 ± 0.06	0.89 ± 0.07	<0.001	<0.001

Supplementary Table 9. Specific experimental data of Figure 5A 5A

Indicator	oe-NC (n=3)	oe-SIX1 (n=3)	*P* value
Relative SIX1 mRNA expression	0.96 ± 0.07	5.76 ± 0.53	0.004

Supplementary Table 10. Specific experimental data of Figure 5B-J

Indicators	si-NC (n=3)	si-GAS5#1 (n=3)	si-GAS5#1+SIX1 (n=3)	*P* value (si-GAS5#1 vs. si-NC)	*P* value (si-GAS5#1+ SIX1 vs. si-GAS5#1)
Cell viability					
24 h	0.28 ± 0.03	0.25 ± 0.03	0.26 ± 0.04	0.483	0.914
48 h	0.79 ± 0.03	0.41 ± 0.04	0.64 ± 0.05	<0.001	<0.001
72 h	1.05 ± 0.07	0.69 ± 0.04	0.88 ± 0.05	<0.001	0.01
96 h	1.59 ± 0.09	1.07 ± 0.08	1.45 ± 0.13	0.002	0.009
ECAR					
5	41.33 ± 1.53	24 ± 2	35 ± 3	<0.001	0.002
10	43.67 ± 1.53	20.33 ± 1.53	35.33 ± 2.09	<0.001	<0.001
15	43.67 ± 3.22	20.67 ± 2.52	35.33 ± 3.51	<0.001	0.003
<0.001	<0.001	28.33 ± 2.08	59.33 ± 3.51	<0.001	<0.001
30	73.67 ± 3.06	31 ± 3.61	67 ± 2	<0.001	<0.001
35	75.33 ± 2.52	31.67 ± 3.51	70 ± 2	<0.001	<0.001
45	117 ± 3.61	65.33 ± 3.06	97.67 ± 4.51	<0.001	<0.001
50	118 ± 2.65	62.33 ± 3.06	105.7 ± 5.86	<0.001	<0.001
55	118 ± 2	59 ± 4	108.7 ± 3.51	<0.001	<0.001
65	25.67 ± 2.08	23 ± 2	25.67 ± 3.06	0.424	0.424
70	26.33 ± 0.58	22 ± 2	19.33 ± 1.53	0.03	0.15
75	22.67 ± 0.58	17.33 ± 1.53	22 ± 2	0.011	0.020
OCR					
5	95 ± 1	109 ± 3	104 ± 2.08	<0.001	0.088
10	94.67 ± 3.79	103.3± 1.53	100.3 ± 3.51	0.033	0.505
15	93.67 ± 2.52	112 ± 4.58	103 ± 4	0.003	0.062
25	45.33 ± 1.53	83.33 ± 1.53	61.67 ± 6.51	<0.001	0.001
30	47 ±3.61	79.33 ± 7.57	59.33 ± 3.51	<0.001	0.008
35	53 ± 2	78 ± 5	58.67 ± 4.16	<0.001	0.002
45	158.7 ± 7.51	251.7 ± 8.02	195.3 ± 5.51	<0.001	<0.001
50	159.3 ± 5.69	236.3 ± 6.11	189.7 ± 3.06	<0.001	<0.001
55	152 ± 3	234.7 ± 6.11	192 ± 4	<0.001	<0.001
65	30.33 ± 2.52	35.33 ± 3.06	37.33 ± 3.06	0.166	0.689
70	29 ± 3	33 ± 2.65	38 ± 3.61	0.325	0.201
75	28.33 ± 3.06	31 ± 2	30.33 ± 2.52	0.46	0.95
Glycolysis capacity	74.78 ±3.80	40.56 ± 3.09	68.78 ± 7.46	<0.001	<0.001
Relative ATP levels	0.97 ± 0.06	0.27 ± 0.06	0.86 ± 0.07	<0.001	<0.001
Maximal respiration	62.22 ± 5.63	132.8 ± 10.73	89.78 ± 2.05	<0.001	<0.001
Relative glucose uptake	99.2 ± 12	39.4 ± 5.5	79.3 ± 8.5	<0.001	0.004
Relative lactate production	1.0 ± 0.1	0.37 ± 0.05	0.82 ± 0.08	<0.001	0.001

Supplementary Table 11. Specific experimental data of Figure 6B

Indicators	Anti-IgG (n=3)	Anti-Ago2 (n=3)	*P* value
Relative enrichment of GAS5	0.92 ± 0.1	87.2 ± 6.8	0.002
Relative enrichment of miR-23a-3p	1.04 ± 0.08	54.5 ± 4.9	0.003

Supplementary Table 12. Specific experimental data of Figure 6C, E

Indicators	NC mimic (n=3)	miR-23a-3p mimic (n=3)	*P* value
Relative miR-23a-3p expression	1.0 ± 0.07	5.54 ± 0.25	<0.001
Relative enrichment of miR-23a-3p	1.04 ± 0.08	54.5 ± 4.9	0.003
Relative luciferase activity			
Wt	1.0 ± 0.10	0.33 ± 0.06	0.001
Mut	0.98 ± 0.09	0.94 ± 0.05	0.499

Supplementary Table 13. Specific experimental data of Figure 6F, M

Indicators	si-NC (n=3)	si-GAS5#1	si-GAS5#2	*P* value (si-GAS5#1 vs si-NC)	*P* value (si-GAS5#2 vs si-NC)
Relative miR-23a-5p expression	0.94 ± 0.08	4.69 ± 0.42	4.32 ± 0.36	0.003	0.003
Relative SLC7A11 expression	1.04 ± 0.06	0.36 ± 0.05	0.41 ± 0.06	<0.001	<0.001

Supplementary Table 14. Specific experimental data of Figure 6H

Indicators	Bio-NC (n=3)	Bio-miR-23a-3p (n=3)	*P* value
Relative SLC7A11 enrichment	0.96 ± 0.08	85.23 ± 7.26	0.003

Supplementary Table 15. Specific experimental data of Figure 6J-K

Indicators	NC mimic (n=3)	miR-23a-3p mimic (n=3)	*P* value
Relative luciferase activity			
Wt	1.05 ± 0.05	0.33 ± 0.07	<0.001
Mut	0.99 ± 0.06	1.03 ± 0.04	0.425
Relative SLC7A11 expression	1.0 ± 0.09	0.22 ± 0.06	<0.001

Supplementary Table 16. Specific experimental data of Figure 6N

Indicators	oe-NC (n=3)	oe-GAS5	oe-GAS5+miR-23a-3p mimic (n=3)	*P* value (oe-GAS5 vs. oe-NC)	*P* value (oe-GAS5+miR-23a-3p mimic (n=3) vs. oe-GAS5)
Relative SLC7A11 expression	1.04± 0.09	5.66 ± 0.54	1.22 ± 0.26	<0.001	<0.001

Supplementary Table 17. Specific experimental data of Figure 7A-F

Indicators	Control (n=3)	Erastin (n=3)	Erastin + oe-NC (n=3)	Erastin + oe-GAS5 (n=3)	Erastin + oe-GAS5+si-SLC7A11 (n=3)	*P* value (Erastin vs. Control)	*P* value (Erastin + oe-GAS5 vs. Erastin+oe-NC)	*P* value (Erastin+oe-GAS5+si-SLC7A11 vs. Erastin+oe-GAS5
Cell viability	1.04 ± 0.05	0.17 ± 0.05	0.15 ± 0.05	0.75 ± 0.05	0.39 ± 0.05	<0.001	<0.001	<0.001
Relative Fe^{2+} level	0.99 ± 0.07	3.02 ± 0.14	2.93 ± 0.13	1.36 ± 0.14	2.67 ± 0.08	<0.001	<0.001	<0.001
MDA level	4.07 ± 1.17	42.5 ± 2.81	41.23 ± 3.3	18.7 ± 1.35	31.17 ± 2.97	<0.001	<0.001	<0.001
Relative GSH/GSSG level	0.98 ± 0.06	0.18 ± 0.04	0.22 ± 0.04	0.85 ± 0.05	0.43 ± 0.07	<0.001	<0.001	<0.001
Relative ROS level	1.04 ± 0.04	4.84 ± 0.10	5.04 ± 0.11	2.3 ± 0.18	4.55 ± 0.14	<0.001	<0.001	<0.001
LDH release	1 ± 0.05	2.47 ± 0.13	2.49 ± 0.14	1.23 ± 0.11	2.3 ± 0.11	<0.001	<0.001	<0.001

Supplementary Table 18. Specific experimental data of Supplementary Figure 1A

Indicators	si-NC (n=3)	si-GAS5#1	si-GAS5#2	*P* value (si-GAS5#1 vs. si-NC)	*P* value (si-GAS5#2 vs. si-NC)
C-Myc	0.96 ± 0.1	1.02 ± 0.09	1.07 ± 0.08	0.483	0.214
SIX1	1.04 ± 0.1	0.32 ± 0.04	0.29 ± 0.05	0.003	0.002
HIF-1	1.08 ± 0.1	0.95 ± 0.09	1.03 ± 0.06	0.170	0.507

Supplementary Table 19. Specific experimental data of Supplementary Figure 2B

Indicators	Control (n=3)	CHD (n=3)	*P* value
hsa-miR-452-5p	1±0.08	0.95±0.06	0.439
hsa-miR-485-5p	0.95±0.06	0.99±0.06	0.460
hsa-miR-31-5p	0.99±0.07	1.07±0.07	0.234
hsa-miR-222-3p	1.02±0.05	1±0.07	0.710
hsa-miR-221-3p	1±0.09	1.1±0.06	0.195
hsa-miR-361-5p	0.99±0.06	1.03±0.08	0.529
hsa-miR-26b-5p	0.94±0.08	1.07±0.06	0.093
hsa-miR-26a-5p	1.03±0.07	1.09±0.06	0.324
hsa-miR-579-3p	0.97±0.06	1.1±0.06	0.057
hsa-miR-23a-3p	1±0.08	5.69±0.45	0.002
hsa-miR-23b-3p	1.04 ±0.06	1.05±0.06	0.848
hsa-miR-136-5p	0.96 ±0.06	3.23±0.45	0.012
hsa-miR-128-3p	0.98±0.08	0.86±0.08	0.140
hsa-miR-876-5p	1.05±0.06	0.92±0.06	0.057
hsa-miR-205-5p	1.04±0.08	0.95±0.08	0.240
hsa-miR-188-5p	0.92±0.06	3.95±0.3	0.002
hsa-miR-382-3p	1.06±0.07	1.02±0.07	0.523
hsa-miR-18a-5p	1.08±0.05	1.1±0.08	0.735
hsa-miR-18b-5p	1.03±0.06	1.08±0.08	0.439
hsa-miR-29a-3p	1.02±0.07	0.89±0.05	0.065
hsa-miR-29b-3p	0.94±0.07	0.84±0.07	0.135
hsa-miR-29c-3p	1.07±0.08	0.9±0.07	0.051

Supplementary Table 20. Specific experimental data of Supplementary Figure 2C

Indicators	Bio-NC (n=3)	Bio-GAS5 (n=3)	*P* value
miR-23a-3p	1.0 ± 0.08	55.62 ± 5.26	0.003
miR-136-5p	0.95 ± 0.08	1.10 ± 0.06	0.065
miR-188-5p	1.03 ± 0.07	0.98 ± 0.06	0.402